

Tree species classification from hyperspectral data using graph-regularized neural networks

Debmata Bandyopadhyay and Subhadip Mukherjee

Abstract—Manual labeling of tree species remains a challenging task, especially in tropical regions, owing to inaccessibility and labor-intensive ground-based surveys. Hyperspectral images (HSIs), through their narrow and contiguous bands, can assist in distinguishing tree species based on their spectral properties. Therefore, automated classification algorithms on HSI images can help augment the limited labeled information and generate a real-time classification map for various tree species. Achieving high classification accuracy with a limited amount of labeled information in an image is one of the key challenges that researchers have started addressing in recent years. We propose a novel graph-regularized neural network (GRNN) algorithm that encompasses the superpixel-based segmentation for graph construction, a pixel-wise neural network classifier, and the label propagation technique to generate an accurate classification map. GRNN outperforms several state-of-the-art techniques not only for the standard Indian Pines HSI but also achieves a high classification accuracy (approx. 92%) on a new HSI data set collected over the forests of French Guiana (FG) even when less than 1% of the pixels are labeled. We show that GRNN is not only competitive with the state-of-the-art semi-supervised methods, but also exhibits lower variance in accuracy for different number of training samples and over different independent random sampling of the labeled pixels for training.

Index Terms—Hyperspectral imaging, forest species classification, neural networks, graph-learning.

I. INTRODUCTION

HYPERSPECTRAL image (HSI) with the several hundred spectral bands capture the entire light distribution through dedicated sensors, providing a detailed spatial and spectral information about the targets. The applicability of this data set ranges from water resource management [1] to forest monitoring [2], object detection [3] to object tracking [4].

Recent studies that have focused on spectral classification methods include neural networks (NN) [5], generative adversarial networks (GANs) for remote sensing [6], apart from the classical support vector machine (SVM) [7] and random forest (RF) [8] technique. Although the supervised learning algorithms for image classification show promising results [9], these methods are heavily reliant on large high-quality labeled training data sets. For real time data, the ground-truth labels are very limited owing to the highly intensive field survey required, especially in inaccessible areas such as dense tropical forests. Semi-supervised learning has successfully tackled the problem of small amount of labeled samples and is able to

extract useful information from both labeled and unlabeled pixels in an image [10]. Furthermore, using hyperspectral data involves dealing with a high-resolution spectral-spatial information with a high dimensional data set. To derive useful information and deal with the high dimensionality, various feature extraction methods like the image fusion and recursive filter by Kang et al. [11], the utilization of local binary patterns by Li et al. [12], the local matrix representation by Fang et al. [13] and the hyper-manifold simple linear iterative clustering combined with the graph learning technique by Sellars et al. [9] have been reported previously. Image classification using neural networks involving both shallow and deep networks [14, 15], have been particularly been useful in efficiently working with limited ground-truth data and class imbalance, alongside learning spatial features from the unlabeled classes to generate a more realistic classification map. However, we need to strike the right balance between computational complexity and the objective of learning from sparsely labeled data from a high-dimensional HSI.

In this letter, we propose a novel graph-regularized neural network (GRNN) classifier which is designed to address three objectives: (i) combine the pixel-based classification and superpixel feature-based learning to extract maximum information from both labeled and unlabeled pixels in the HSI and (ii) generate an accurate and realistic classification map by jointly optimizing the accuracy of the NN and a graph energy potential that seeks to promote smoothness in the predicted classification map. Finally, the NN output predictions (exceeding a certain confidence) are used to augment the ground-truth labels, on which we apply the classical semi-supervised label propagation method [16] using the superpixel graph to generate the final classification map. Precise mathematical details of GRNN and our experimental findings are reported in Sections II and III, respectively.

II. PROPOSED METHOD

The key idea behind the proposed graph-regularized neural network (GRNN) classification approach is to use a pixel-wise fully-connected NN classifier in conjunction with a superpixel graph to learn effectively from few labeled pixels and a large number of unlabeled pixels. The output probability distribution of the NN is regularized using a graph-based energy functional that essentially encourages a smooth variation of the NN output on the superpixel graph. The details of the GRNN algorithm are explained in the following, and a schematic of the entire pipeline is shown in Figure 1.

The given HSI image $X \in \mathbb{R}^{H \times W \times B}$, having spatial resolution $H \times W$ and B spectral bands, is first reduced via

Debmata Bandyopadhyay (corresponding author), is with the Department of Plant Sciences, University of Cambridge, CB2 3EA, United Kingdom, e-mail: b.debmata@gmail.com.

Subhadip Mukherjee is with the Department of Applied Mathematics and Theoretical Physics, University of Cambridge, CB3 0WA, United Kingdom.

PCA to $x \in \mathbb{R}^{H \times W \times b}$, where $b \ll B$. The number of bands b is chosen such that 99.90% of variance in the HSI data is preserved. The labeled and unlabeled pixels in the given HSI image are denoted by \mathcal{L} and \mathcal{U} , respectively.

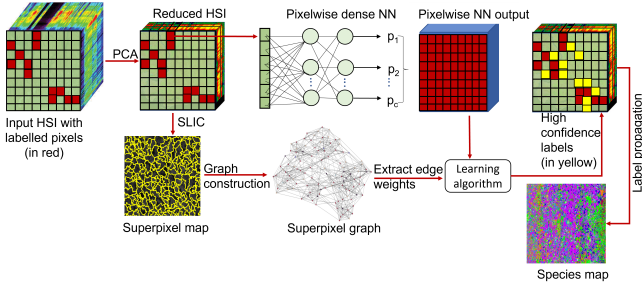


Fig. 1: Framework for the proposed method, GRNN.

Following PCA, we apply the SLIC algorithm [17] to the first principal component of X to extract N superpixels, denoted as $\{\mathcal{S}_k\}_{k=1}^N$, which are subsequently utilized to construct a graph. An essential step for superpixel graph construction is feature extraction, for which we follow the same procedure outlined in [9, Sec. III.B]. The nodes of the graph so constructed represent the superpixels and the adjacency weights $W_{k\ell}$ capture the similarity between superpixels \mathcal{S}_k and \mathcal{S}_ℓ in terms of the extracted features. We follow the same procedure as reported in [9] for constructing the graph adjacency matrix $W \in \mathbb{R}^{N \times N}$. Small adjacency weights are set to 0 by retaining only the top N_s elements in each row of W . This thresholding step sparsifies W and leads to efficient training. We choose $N_s = 20$ in our experiments, i.e., each node can have at most 20 neighboring nodes. A superpixel \mathcal{S}_k is said to be labeled if it contains at least one labeled pixel in it, i.e., $\mathcal{S}_k \cap \mathcal{L} \neq \emptyset$, and the set of all labeled superpixels is denoted as \mathcal{L}^{sp} . For a c -class classification problem, let $y_i \in \{1, 2, \dots, c\}$ be the true label of any pixel $\mathbf{i} = (i_1, i_2) \in \mathcal{L}$. The one-hot encoding of y_i is denoted by $Y_i \in \mathbb{R}^c$, and is defined as follows, where $q \in \{1, 2, \dots, c\}$:

$$Y_i(q) = \begin{cases} 1 & \text{if } y_i = q \\ 0 & \text{if } y_i \neq q. \end{cases} \quad (1)$$

For any labeled superpixel $\mathcal{S}_k \in \mathcal{L}^{\text{sp}}$, we compute two labels, referred to as the soft- and the hard label, respectively. The soft label $t_{\mathcal{S}_k}$ represents the relative frequency of different classes within it, and is computed as $t_{\mathcal{S}_k} = \frac{1}{|\mathcal{S}_k \cap \mathcal{L}|} \sum_{\mathbf{j} \in \mathcal{S}_k \cap \mathcal{L}} Y_{\mathbf{j}}$. Note that for any $\mathcal{S}_k \in \mathcal{L}^{\text{sp}}$, the soft label $t_{\mathcal{S}_k} \in \Delta_c$, where Δ_c is the probability simplex in \mathbb{R}^c . The hard label $T_{\mathcal{S}_k}$ corresponding to \mathcal{S}_k represents the most frequent class in \mathcal{S}_k using a one-hot encoding. Specifically, $T_{\mathcal{S}_k} \in \mathbb{R}^c$ is a c -length vector whose q_*^{th} element is 1, and every other element is 0, where $q_* = \arg \max_{q \in \{1, 2, \dots, c\}} t_{\mathcal{S}_k}(q)$. For unlabeled superpixels, i.e., for $\mathcal{S}_k \notin \mathcal{L}^{\text{sp}}$, both $t_{\mathcal{S}_k}$ and $T_{\mathcal{S}_k}$ are defined as c -length vectors with all zeros. Let, $T^{(\mathcal{L})}$ be the $N \times c$ matrix whose k^{th} row is $T_{\mathcal{S}_k}$. The superscript \mathcal{L} is used to indicate explicitly that T depends on the underlying set of labeled pixels \mathcal{L} .

Besides the superpixel graph, the other key component of GRNN is a pixel-wise, fully-connected NN-based classifier

$\phi_\theta : \mathbb{R}^b \mapsto \Delta_c$ with parameters θ . The NN has two intermediate layers with leaky-ReLU activations (with negative slope 0.1)¹ and a softmax layer in the end. The output of the NN gives a probability map over c classes, i.e., for any pixel location $\mathbf{i} \in \mathbb{R}^2$, $\phi_\theta(x_{\mathbf{i}}) \in \Delta_c$ represents the predicted probabilities of the pixel belonging to any of the c classes. The predicted probability map for a superpixel is computed by averaging the probability maps of all the pixels within the given superpixel: $\phi_{\mathcal{S}_k} = \frac{1}{|\mathcal{S}_k|} \sum_{\mathbf{j} \in \mathcal{S}_k} \phi_\theta(x_{\mathbf{j}})$. The overall training loss seeks to simultaneously achieve the following objectives: (i) minimize classification errors, both for the pixels and the superpixels for which the ground-truth labels are available, (ii) ensure that the predicted superpixel probability map varies smoothly over the graph, (iii) minimize the variance in the predicted pixel-wise probability maps within each superpixel, and (iv) discourage uniform labeling of the unlabeled superpixels, i.e., make sure that all unlabeled superpixels do not end up with the same predicted class and that all classes are represented overall. To accomplish these objectives, the training problem is formulated as

$$\begin{aligned} \min_{\theta} \left[\sum_{\mathbf{j} \in \mathcal{L}} \mathcal{D}_1(Y_{\mathbf{j}}, \phi_\theta(x_{\mathbf{j}})) + \lambda_{\text{spc}} \sum_{k: \mathcal{S}_k \in \mathcal{L}^{\text{sp}}} \mathcal{D}_2(t_{\mathcal{S}_k}, \phi_{\mathcal{S}_k}) \right. \\ \left. + \lambda_g \sum_{\mathcal{S}_k, \mathcal{S}_\ell} \left\| \frac{\phi_{\mathcal{S}_k}}{\sqrt{d_k}} - \frac{\phi_{\mathcal{S}_\ell}}{\sqrt{d_\ell}} \right\|_2^2 + \lambda_v \sum_{\mathcal{S}_k} \text{var} \{ \phi_\theta(x_{\mathbf{j}}) \}_{\mathbf{j} \in \mathcal{S}_k} \right. \\ \left. - \lambda_{\text{en}} \mathcal{H} \left(\frac{1}{N} \sum_{k=1}^N \phi_{\mathcal{S}_k} \right) \right]. \quad (2) \end{aligned}$$

Here, $d_k = \sum_{\ell \neq k} W_{k\ell}$ denotes the degree of node- k of the superpixel graph, \mathcal{D}_1 and \mathcal{D}_2 measure pixel- and superpixel-wise classification losses, respectively, and $\mathcal{H} : \Delta_c \mapsto \mathbb{R}$ denotes the entropy functional. The first two terms in (2) promote high classification accuracy on the labeled pixels and superpixels, respectively. We choose \mathcal{D}_1 to be the cross-entropy loss, while \mathcal{D}_2 is taken as the standard squared Euclidean distance. The third term is a graph energy function which imposes a smoothness prior on the predicted superpixel probability map, ensuring that it does not vary abruptly as a function defined on the superpixel graph. The fourth term in the training loss seeks to minimize the variance of prediction probabilities for all pixels inside each superpixel, which promotes high intra-superpixel similarity of the predicted class. The final negative entropy term penalizes a uniform labeling of the unlabeled superpixels, thereby encouraging high inter-superpixel variability of the predicted classification map. The λ parameters associated with different terms in the overall training loss trade-off different components of the loss functional and need to be selected optimally. The training problem (2) is solved iteratively using the Adam optimizer [18], the de facto standard for training NNs, with a learning rate of 10^{-3} , and $(\beta_1, \beta_2) = (0.9, 0.999)$.

The trained NN, although optimized simultaneously for accuracy and low intra-superpixel variability of the classification map, can still produce a classification map with differently labeled pixels inside same superpixels. Such a prediction might

¹leaky-relu(u) = max(0, u) + γ min(0, u), where γ = negative slope.

be physically unrealistic, since the superpixels are generated based on spectral similarity and any given superpixel should ideally belong to a single tree species. To circumvent this, the final step of GRNN generates a smooth label map by applying the classical label propagation algorithm for semi-supervised learning on graphs [16], after combining the NN prediction with the ground-truth labels. The label propagation step is carried out by augmenting the given ground-truth labels with the labels predicted by the NN with high-confidence. The set of pixels for which the trained NN classifies with confidence exceeding a given threshold $\tau \in (0, 1)$ is defined as

$$\mathcal{I} = \{\mathbf{i} : \max(\phi_{\theta^*}(x_i)) \geq \tau\}, \quad (3)$$

where θ^* is the optimal set of NN parameters obtained by solving (2). In other words, if the probability of the most likely class is greater than τ then the corresponding predicted label is added to the existing ground-truth labels. We set $\tau = 0.4$ in our experiments. The smoothed superpixel probability map is generated by

$$T^* = \left(\text{Id} - \alpha D^{-\frac{1}{2}} W D^{\frac{1}{2}}\right)^{-1} T^{(\mathcal{M})}, \quad (4)$$

where Id denotes the $N \times N$ identity matrix, $T^{(\mathcal{M})}$ is the $N \times c$ one-hot superpixel probability matrix computed using the augmented set of labeled pixels given by $\mathcal{M} = \mathcal{L} \cup \mathcal{I}$, and $W \in \mathbb{R}^{N \times N}$ and $D \in \mathbb{R}^{N \times N}$ are the graph adjacency and the (diagonal) degree matrices, respectively. For any superpixel S_k , the final classification label is produced as $q_k = \arg \max_{q \in \{1, 2, \dots, c\}} T_{S_k}^*(q)$, where $T_{S_k}^*$ is the k^{th} row of T^* . All pixels within a superpixel are assigned the same class label as their parent superpixel.

III. EXPERIMENT AND RESULTS

1) *Data description/set up:* From the widely used HSI data sets, Indian Pines (IP) is utilized to compare the proposed method with the existing state-of-the-art classification techniques. The IP data set consists of 224 bands, 16 classes and has a spatial resolution of 20 m (with 145×145 pixels). The data was collected over an agricultural site by the airborne visible/infrared imaging spectrometer (AVIRIS) sensor. To check the robustness of the novel method, we apply the GRNN algorithm to a new data collected with Hypex VNIR-1600 sensor-mounted alongside the Riegl scanner. The study site is Paracou ($5^\circ 18' \text{N}$, $52^\circ 55' \text{W}$) in French Guiana (FG), which is a tropical rain forest. The data set comprises 374 bands, 76 tree species with 1 m spatial resolution [19] (consisting of 668×923 pixels). The ground truth labels were manually confirmed from field survey and the crowns manually segmented using the QGIS open-source software. Only the top-10 most dominant species were considered for classification and the other species were excluded.

Our experiment is performed in two stages. First, we develop and test the algorithm on the benchmark IP HSI data and compare the performance in terms of overall accuracy (OA) and the Cohen kappa coefficient (κ) with competing classification methods. Subsequently, we test GRNN on the large-scale, highly heterogeneous FG HSI data with very

limited ground-truth labels. Among the labeled pixels, the test and training samples were randomly chosen to estimate the OA and the κ coefficient. The mean and standard deviation in classification accuracy were evaluated over ten random trials for the benchmark HSI data.

2) *Hyperparameter selection:* GRNN involves two sets of hyperparameters, for graph construction and for training, respectively. Optimal selection of these hyperparameters is of crucial importance for the success of GRNN. The specific values chosen for the hyperparameters corresponding to two different data sets in our experiments are reported in Table I. A principled approach to learn these hyperparameters from the data would be highly desirable, and we leave it as a future work.

TABLE I: The hyperparameters for graph construction and GRNN. h , β , σ_s and σ_l are as defined in equations (5), (8), and (9) in [9]. ξ is the connectivity parameter that defines superpixel adjacency, which required for feature extraction. n_θ represents the total number of NN parameters. N is the number of superpixels extracted using SLIC, the λ parameters control different components of the training objective (2), α is the label-smoothing parameter in (4), τ is the threshold in (3), and n_{iter} = number of training iterations.

superpixel graph construction and NN parameters							
	h	β	σ_s	σ_l	ξ	n_θ	
Indian Pines	15.0	0.9	2.0	1.0	8	73888	
French Guiana	15.0	0.5	5.0	40.0	8	369778	
GRNN parameters							
	N	λ_{spc}	λ_g	λ_v	λ_{en}	α	n_{iter}
Indian Pines	1200	0.15	10^5	2.0	20.0	0.5	500
French Guiana	5000	0.1	0.2	0.1	20.0	0.5	400

3) *Comparison with different methods:* We compare and benchmark the performance of the proposed GRNN framework with respect to several state-of-the-art methods, namely the local covariance matrix representation (LCMR) [13], superpixel-based classification via multiple kernels (SC-MK) [20], edge preserving filter (EPF) [21], local binary pattern (LBP) method [12], the image fusion and recursive filtering (IFRF) [11] and the SVM method [7].

GRNN performs qualitatively (Figure 2) and quantitatively (Table II) better than the existing classifiers for the Indian Pines data set. Specifically, the difference in κ from the nearest competitive algorithm SGL (which is also based on superpixel segmentation and graph-based semi-supervised label propagation) is about 0.08. The key difference between SGL and GRNN is the NN-assisted graph learning which utilizes both pixel- and superpixel-level information for efficient semi-supervised classification. The high-confidence NN predictions are used to augment the set of few available ground-truth labels, and a smooth classification map is generated using the classical label propagation approach [9, 16].

To understand the effect of the amount of labeled samples on the overall accuracy, we compared GRNN with one of the best-performing semi-supervised algorithms (namely, SGL) and the classical supervised method of SVM (Figure 3). It is seen that the OA in all the three methods systematically increases as the number of samples increases from three to fifteen. However, the GRNN does not show much change in accuracy (varies between 95% and 96%) with reduction in number of training

TABLE II: Comparison of different methods on Indian Pines in terms of overall accuracy and the κ score, corresponding to ten number of samples per class. The best scores are highlighted in boldface.

	Ours	SGL	LCMR	SC-MK	EPF	LBP	IFRF	SVM
OA (%)	96.3 \pm 0.8	90.7 \pm 2.2	82.7 \pm 3.1	80.7 \pm 2.5	67.3 \pm 3.2	78.9 \pm 2.7	80.3 \pm 1.8	53.1 \pm 1.9
κ	0.96 \pm 0.01	0.88 \pm 0.03	0.81 \pm 0.03	0.77 \pm 0.03	0.65 \pm 0.02	0.78 \pm 0.02	0.78 \pm 0.04	0.48 \pm 0.02

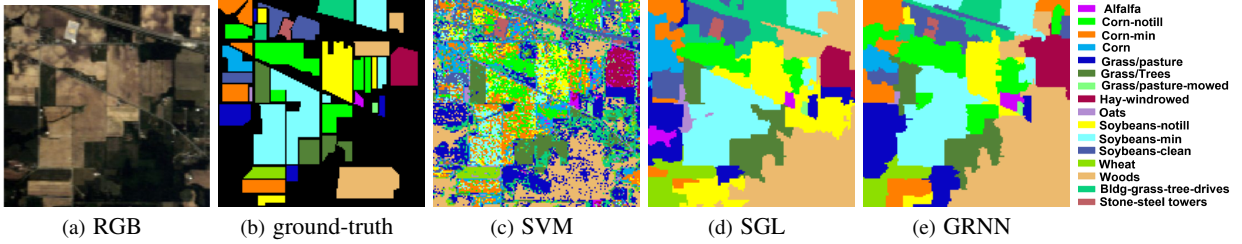


Fig. 2: Comparison of SVM (supervised), SGL (semi-supervised), and the proposed GRNN classification maps on Indian Pines with ten samples per class. Qualitatively, GRNN produces a smoothed classification map with a higher accuracy as reported in Table II.

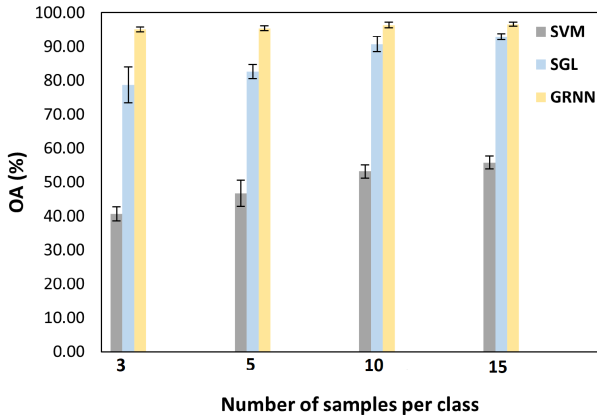


Fig. 3: Comparison of the OA of SVM, SGL and the proposed GRNN-based classification on Indian Pines. The error bar represent the variance in the accuracy after ten iterations on the test samples. GRNN is more robust with higher accuracy as compared to SGL.

samples. It is interesting to note that the variance in the OA for GRNN is also significantly smaller in comparison with the other methods. The value for variance is 0.58 to 0.80 whereas for the other methods the variance is as high as 3.85 for SGL and 5.30 for SVM.

We extend the study to a new study area of French Guiana for which the data has very limited labeled information (even lesser than the standard data). The FG data set has highly heterogeneous classes which change as one moves from one crown to another. Further, there is an imbalance in class representation, and, we, therefore, select the ten most commonly occurring classes to train the model and generate the classification map. The GRNN algorithm after hyperparameter tuning (Table I), is trained using 10%, 30%, 50% and 70% of the labeled data. With 10% of the data, the percentage of pixels used for training is $< 1\%$ considering the total number of pixels in the image. Even with such less labeled information, the algorithm has a κ score of 0.79. As the percentage of training samples is increased, the OA and κ improves up to 0.89. However, the performance plateaus beyond 50%

training data usage. The experiments indicate that GRNN is particularly suitable when very few pixels are labeled.

IV. CONCLUSIONS

We propose a novel algorithm based on superpixel graph energy minimization and a NN classifier for HSI image classification. The algorithm is validated on the standard Indian Pines region and shows an improved performance (varied between 6% and 16% increase in OA) compared to other state-of-the-art semi-supervised methods. The proposed GRNN method is also applied to a new high-resolution highly heterogeneous HSI data set and is consistent in performance (around 85% OA) using just 10% of the training samples (which is $< 1\%$ of the total pixels). GRNN can learn from a limited labeled data set by optimizing the neural network accuracy with a superpixel graph-based energy that imposes a strong prior on the predicted classification map. In addition to the enhanced accuracy, the variance in the estimates is also significantly less compared to other methods. The reduced variance highlights the robustness of the GRNN algorithm with respect to the randomly selected samples for training. In our future work, we intend to explore automatic feature learning from the extracted superpixels instead of using handcrafted features to enhance the performance of GRNN.

Acknowledgment: The Indian Pines data is courtesy of D. Landgrebe, Purdue University, and the NASA Jet Propulsion Laboratory. We thank James Ball from the department of Plant Sciences, University of Cambridge and the CIRAD-Joint Research Unit Ecology of Guiana Forests for sharing the airborne HSI data and annotated tree species information for forests in French Guiana. We would like to thank David A. Coomes and Carola-Bibiane Schönlieb for their technical inputs.

REFERENCES

- [1] P. Qin, Y. Cai, and X. Wang, "Small waterbody extraction with improved u-net using zhuhai-1 hyperspectral remote sensing

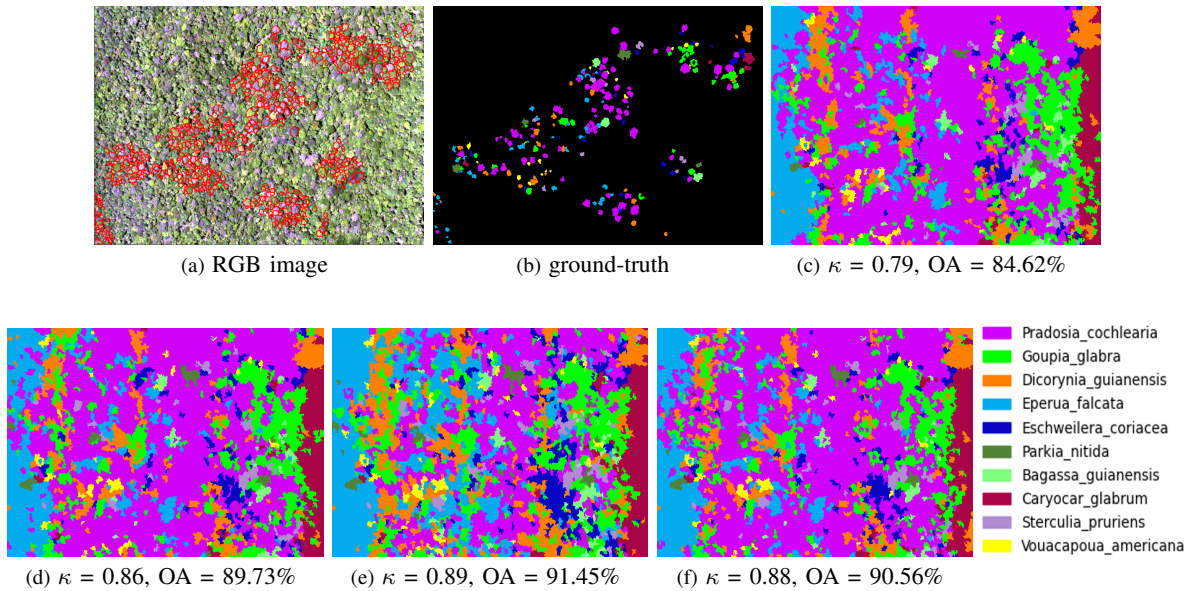


Fig. 4: GRNN applied to the FG data: (a) shows the composite RGB image of the forest region wherein the red polygons are the annotated tree crowns, (b) shows the labeled tree species for which the key is provided in the bottom right corner of the image. GRNN applied on FG with (c) 10%, (d) 30%, (e) 50% and (f) 70% of the available labeled pixels shows the algorithm's ability to learn from very limited ($< 1\%$ of the total number of pixels) labels with a high accuracy. Classification for the ten most frequent species is performed in this experiment.

- images," *IEEE Geoscience and Remote Sensing Letters*, vol. 19, pp. 1–5, 2022.
- [2] M. Mörtus, P. Pham, E. Halme, M. Molinier, H. Cu, and J. Laaksonen, "Taiga: a novel dataset for multitask learning of continuous and categorical forest variables from hyperspectral imagery," *IEEE Transactions on Geoscience and Remote Sensing*, vol. 60, pp. 1–11, 2022.
- [3] Y. Zhang, B. Du, L. Zhang, and T. Liu, "Joint sparse representation and multitask learning for hyperspectral target detection," *IEEE Transactions on Geoscience and Remote Sensing*, vol. 55, no. 2, pp. 894–906, 2016.
- [4] T. Wang, Z. Zhu, and E. Blasch, "Bio-inspired adaptive hyperspectral imaging for real-time target tracking," *IEEE Sensors Journal*, vol. 10, no. 3, pp. 647–654, 2010.
- [5] A. Krizhevsky, I. Sutskever, and G. E. Hinton, "Imagenet classification with deep convolutional neural networks," *Advances in neural information processing systems*, vol. 25, 2012.
- [6] S. Jozdani, D. Chen, D. Pouliot, and B. Alan Johnson, "A review and meta-analysis of generative adversarial networks and their applications in remote sensing," *International Journal of Applied Earth Observation and Geoinformation*, vol. 108, p. 102734, 2022.
- [7] F. Melgani and L. Bruzzone, "Classification of hyperspectral remote sensing images with support vector machines," *IEEE Transactions on Geoscience and Remote Sensing*, vol. 42, no. 8, pp. 1778–1790, 2004.
- [8] L. Breiman, "Random forests," *Machine learning*, vol. 45, no. 1, pp. 5–32, 2001.
- [9] P. Sellars, A. I. Aviles-Rivero, and C. B. Schonlieb, "Superpixel Contracted Graph-Based Learning for Hyperspectral Image Classification," *IEEE Transactions on Geoscience and Remote Sensing*, vol. 58, no. 6, pp. 4180–4193, 2020.
- [10] X. Zhu, "Semi-supervised learning literature survey, dept. computer. sci., univ. wisconsin-madison," Madison, Tech. Rep. 1530, Tech. Rep., 2005.
- [11] X. Kang, S. Li, and J. A. Benediktsson, "Feature extraction of hyperspectral images with image fusion and recursive filtering," *IEEE Transactions on Geoscience and Remote Sensing*, vol. 52, no. 6, pp. 3742–3752, 2013.
- [12] W. Li, C. Chen, H. Su, and Q. Du, "Local binary patterns and extreme learning machine for hyperspectral imagery classification," *IEEE Transactions on Geoscience and Remote Sensing*, vol. 53, no. 7, pp. 3681–3693, 2015.
- [13] L. Fang, N. He, S. Li, A. J. Plaza, and J. Plaza, "A New Spatial-Spectral Feature Extraction Method for Hyperspectral Images Using Local Covariance Matrix Representation," *IEEE Transactions on Geoscience and Remote Sensing*, vol. 56, no. 6, pp. 3534–3546, 2018.
- [14] H. Yu, H. Zhang, Y. Liu, K. Zheng, Z. Xu, and C. Xiao, "Dual-channel convolution network with image-based global learning framework for hyperspectral image classification," *IEEE Geoscience and Remote Sensing Letters*, vol. 19, pp. 1–5, 2022.
- [15] K. Safari, S. Prasad, and D. Labate, "A multiscale deep learning approach for high-resolution hyperspectral image classification," *IEEE Geoscience and Remote Sensing Letters*, vol. 18, no. 1, pp. 167–171, 2021.
- [16] D. Zhou, O. Bousquet, T. Lal, J. Weston, and B. Schölkopf, "Learning with local and global consistency," *Advances in neural information processing systems*, vol. 16, 2003.
- [17] R. Achanta, A. Shaji, K. Smith, and A. Lucchi, "SLIC Superpixels Compared to State-of-the-Art Superpixel Methods," *IEEE Transactions on Pattern Analysis and Machine Intelligence*, vol. 34, no. 11, pp. 2274–2281, 2012.
- [18] D. P. Kingma and J. Ba, "Adam: A method for stochastic optimization," *arXiv:1412.6980v9*, 2014.
- [19] M. Aubry-Kientz, A. Laybros, B. Weinstein, J. G. C. Ball, T. Jackson, D. Coomes, and G. Vincent, "Multisensor data fusion for improved segmentation of individual tree crowns in dense tropical forests," *IEEE Journal of Selected Topics in Applied Earth Observations and Remote Sensing*, vol. 14, pp. 3927–3936, 2021.
- [20] L. Fang, S. Li, W. Duan, J. Ren, and J. A. Benediktsson, "Classification of hyperspectral images by exploiting spectral-spatial information of superpixel via multiple kernels," *IEEE transactions on geoscience and remote sensing*, vol. 53, no. 12, pp. 6663–6674, 2015.
- [21] X. Kang, S. Li, and J. A. Benediktsson, "Spectral-spatial hyperspectral image classification with edge-preserving filtering,"

IEEE transactions on geoscience and remote sensing, vol. 52,
no. 5, pp. 2666–2677, 2013.